Ship-Generated Solitons and the Dynamic Vessel Response as a Function of Blockage

Scott Forrest[1]

Abstract

A vessel travelling at critical Froude depth in specific conditions can produce a cyclic wave phenomenon known as solitons. These waves are unique in that they travel faster than the vessel, however they require very specific conditions, so are very rarely observed under normal circumstances. Physical scale model testing was conducted with a focus on blockage coefficient; a function of vessel draft and channel width. Through the systematic variation of vessel draft and channel width it was determined the amplitude of solitons is observably indistinguishable for nominally equivalent blockage and Froude depth. However, when considering period of soliton generation and resistance, model draft had a more significant influence. Dynamic trim and resistance oscillation periods were quantified to be equal to that of soliton generation. Additionally, an educational multimedia presentation was created with footage and data acquired from the physical scale model testing. Fluorescent paint, rhodamine dye and positively buoyant wax particles were illuminated with ultraviolet (UV-A) lighting to visually enhance the soliton event.

Keywords

Ship-generated solitons, wave wake, blockage coefficient, dynamic response, physical scale model testing, advanced qualitative techniques, fluorescence, ultraviolet lighting, web-based educational multimedia tool

1 Introduction

A moving disturbance travelling on the surface of a body of water will create a pattern of waves which is governed by the conditions of the vessel and the environmental surroundings. The predominant factor governing the waves a vessel generates is the Froude depth number, Fr_h, a non-dimensional parameter dependent on vessel speed, u, and water depth, h (Eq. 1).

$$Fr_h = \frac{u}{\sqrt{gh}} \tag{1}$$

The Froude depth number separates vessel-generated waves into three implicit regions, the sub-critical region, more commonly referred to as the deep water or Kelvin wave pattern, the trans-critical region and the super-critical region (Macfarlane, 2012). The sub-critical wave pattern has been investigated extensively and the waves produced within this region account for the vast majority of waves produced by vessels in normal operating conditions. The trans-critical wave pattern is not as well defined, particularly as the vessel approaches 'critical' speed. In open water, the

[1] Scott Forrest:
Bachelor of Engineering (Naval Architecture) (Honours)
email: forrests@utas.edu.au
NCMEH, University of Tasmania, Australian Maritime College, University of Tasmania

speed of a wave is limited by the depth of the water, at less than $Fr_h = 0.56$, the vessel will generate a typical Kelvin wake, a combination of divergent and transverse waves. The location where the two waves meet is termed the 'cusp'. For a Kelvin wake, the transverse and diverging waves form a cusp angle, α, of 19°28' (Figure 1). As the vessel speed increases beyond $Fr_h = 0.56$, the cusp angle forming a typical Kelvin wake will diverge away from the vessel. The diverging effects aren't visible until beyond $Fr_h=0.7$ (α = 20°18'), where cusp angle dramatically diverges towards a theoretical value of 90° at critical vessel speed equal to √(gh), at which point $Fr_h = 1$ (Havelock, 1908). When a vessel reaches critical Froude depth, the transverse waves dissipate and a perpendicular wave front that travels with the vessel develops. According to first order linear theory, this perpendicular wave will grow in amplitude towards infinity, however in practice the amplitude is restricted by dispersion and non-linearity, and the wave will grow laterally at a rate equal to vessel speed (Gourlay, 2010). When a vessel passes through the critical region into super-critical, the transverse waves are no longer produced due to the wave speed limit of water depth, and the waves become long-crested in contrast to the shorter-crested waves of the sub-critical wave pattern (Macfarlane et al., 2014). The transition between the Froude depth regions is illustrated in Figure 1.

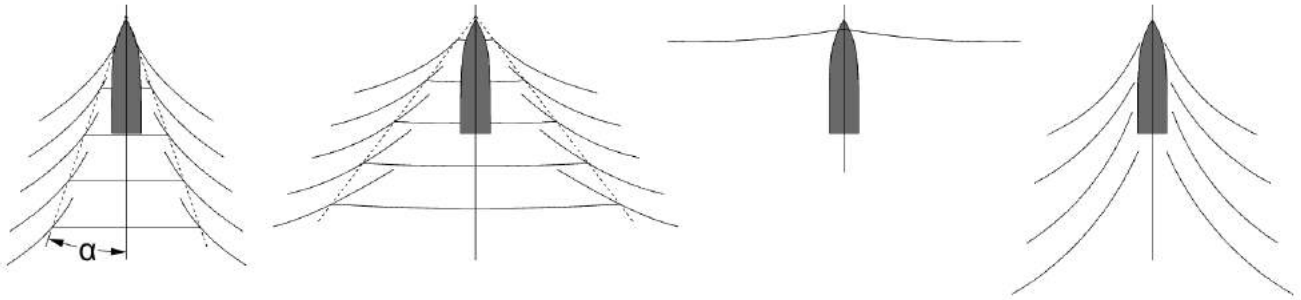

Figure 1: Wave patterns generated by a vessel at varying Froude depth

Travelling at critical speed is also accompanied by a peak in wave-making resistance, sinkage and trim. However, these observations are confined to predicting the wave wake of a vessel travelling in an unbounded domain.

If a vessel is travelling at critical Froude depth number in a laterally bounded waterway, such as in a channel, the perpendicular wave crest cannot grow laterally and the restrained energy disperses ahead of the vessel periodically in the form of two-dimensional waves known as solitons (Ertekin et al., 1985). In practice, solitons are not generated solely at critical Froude depth, but over a range of the trans-critical region from approximately $Fr_h = 0.7$ up to $Fr_h = 1.2$, at which point the soliton breaks and becomes a bore wave. If a vessel continues to operate at a soliton-generating Froude depth, which is very unlikely in reality, solitons will be generated periodically as a continuous oscillation indefinitely, until the vessel or surrounding conditions are no longer sufficient to produce solitons. As Froude depth increases in the trans-critical region, the generated solitons increase in amplitude, speed and energy, and decrease in period, until the onset of a bore wave (Robbins et al., 2011). The extent of this range is determined by blockage coefficient, *m*, a relationship between vessel midship area and channel sectional area, as illustrated in Figure 2.

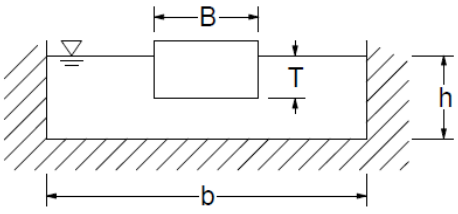

Figure 2: Cross-section illustrating blockage, *m*

Blockage has been determined as the dominant parameter governing soliton generation and not only defines when solitons are produced but also the amplitude, speed, period and energy of the solitons (Ertekin et al., 1984). Ertekin determined that similarly to Froude depth, increasing blockage coefficient also results in increased soliton amplitude and speed, and a decrease in period.

The increased resistance and trim encountered when operating at critical Froude depth is steady for an unrestricted waterway, however when a vessel is generating solitons the wave-making resistance and trim fluctuate as solitons are generated. The increase in resistance when solitons are being generated is likely to present a virtual barrier for ships and speed is unlikely to be maintained. However, for a towed model, after initial acceleration, the oscillations will become 'steady' in that each oscillation is indistinguishable from the previous one, and the higher the initial acceleration, the earlier the oscillations approach a steady mean value (Robbins et al., 2009).

Travelling at trans-critical speed is unrealistic for the majority of vessels, however with a global increase in fast ferry transport vessels, operating in this region is becoming more common (Dand et al., 1999). The implications of travelling at trans-critical speed are not only an increase in trim and resistance for the vessel, solitons themselves have a shape such that they can travel large distances with relatively unchanged form (Gourlay, 2010). Restricted waterways are often associated with areas of high activity, and waves that travel large distances with constant amplitude are an obvious hazard to infrastructure, smaller vessels, and banks due to erosion. An instance was recorded where the high speed ferry *HSS Stena Discovery* passed thorough the Froude depth critical region, generating a high energy wave which grew to a reported height of 4m and swamped the fishing vessel *Purdy*, resulting in a fatality (MAIB, 2000). Despite the undesirable and potentially damaging consequences of travelling in the trans-critical region and producing solitons, general knowledge is minimal (Macfarlane, 2016).

A subsequent outcome of this study is the creation and implementation of a web-based educational tool involving computer-generated imagery, footage from multiple model mounted high-definition recording devices and data from physical scale model testing. Unambiguously capturing the free-surface can be challenging in an environment of bright lighting and mirror-like reflective water surfaces. A method of eliminating glare and reflections and increasing contrast is to illuminate only the model with fluorescent paint and the free-surface with fluorescent wax particles and rhodamine dye activated using ultra-violet (UV-A) lighting (Geerts et al., 2011).

The present study intends to experimentally investigate the variables comprising blockage coefficient to manipulate solitons and investigate the model response as solitons are generated. Subsequently advanced qualitative techniques and recorded footage will be synthesised into a publically accessible web-based educational multimedia tool.

2 Methodology

A series of physical scale model experiments to replicate solitons were conducted in the Australian Maritime College Model Test Basin. The water depth and channel width were controlled to simulate the generalised rectangular cross section depicted in Figure 2. The model test basin is 35m long, 12m wide, has a depth range of 0 to 1m and the bottom of the basin is flat to within ±3mm. The testing conditions were achieved by installing false channel walls using galvanised steel sheets and railway iron sections, and were placed lengthwise along the basin at the required transverse locations. The water depth remained constant for the entirety of testing at h = 152mm. A wave-damping beach setup was required at the end of the channel as solitons lose minimal energy when reflecting off a solid vertical surface. The width of the channel could be altered by relocating the vertical walls where required, and the model remained centred between the two channel walls. Channel widths of 2.0m and 2.36m were selected to produce comparable blockage coefficients for the given vessel drafts. The ship model selected for testing was AMC Model 96-18, a 2.12m long wall-sided monohull full-form bulk-carrier (MarAd F Series) with $C_B = 0.85$, beam, B = 364mm, drafts, T = 61mm, 76mm and 91.5mm and a midship area coefficient of ~0.98 to maximise blockage (Roseman, 1987).

The model was free to heave and pitch and was towed over a distance of 25m attached to a carriage travelling along a rail system capable of speeds up to 3.6 m/s. All instrumentation besides the static wave probes was attached to the carriage and transferred data to the data acquisition system wirelessly. The carriage mounted instrumentation included forward and aft Linear Variable Differential Transformers (LVDTs) to record vertical motion and trim of the model and a load cell to record resistance. Three static wave probes were positioned in the latter half of the channel parallel to the sailing line, and spaced 3.5m apart to quantify Water Surface Elevation (WSE) to indicate soliton development and speed. The wave probes were located at a transverse distance of 860mm from the centreline of the model and the location of the wave probes remained constant throughout testing. The water surface elevation, resistance force and vertical location of bow and stern of the model were digitally recorded with a frequency of 200Hz several seconds

prior to accelerating, until several seconds after the vessel had come to rest. A general layout of the experimental set up can be seen in Figure 3.

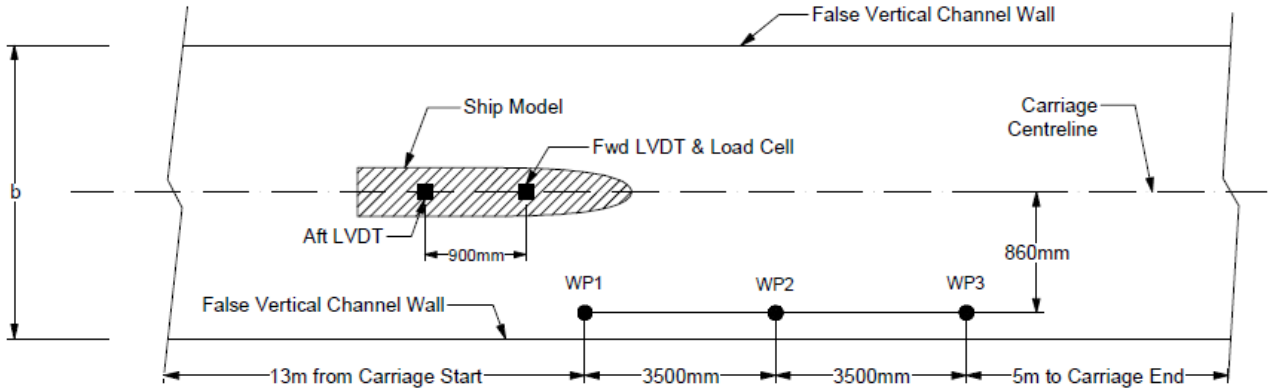

Figure 3: Model test basin arrangement during physical scale model testing

The model accelerated for 2m to ensure steady state speed was reached as early as possible without placing excessive strain on the equipment, and the deceleration ramp rate was 0.30ms^{-2} to ensure the following wake did not swamp the stern of the model.

2.1 Testing Program

The testing program was designed to cover the Froude depth range from sub-critical, through trans-critical, and into super-critical; intending to capture the entire spectrum of soliton generation for each blockage condition. Blockage was varied via vessel draft and channel width, allowing systematic increase in blockage with comparable pairs of nominally equivalent blockages that are comprised of different model drafts and channel widths. The details of the test program are provided in Table 1. Conditions (1) and (5) have a common nominal blockage ratio of 0.075 and Conditions (2) and (6) a blockage ratio of 0.092. Each testing condition covered a minimum Froude depth range of 0.7 to 1.05 resulting in approximately 65 data collecting runs. Upon completion of the test program, an optimal condition to represent solitons was selected, the data-collecting instrumentation was removed, and the focus was placed on manipulating the fluorescent media and array of ultraviolet lighting for qualitative video capture.

Table 1: AMC Model Test Basin testing conditions

Vessel Draft / **Channel Width**	T = 61 mm	T = 76 mm	T = 91.5 mm
2.0 m	**(1)** Blockage, *m* = **0.073** Fr_h = 0.7 – 1.1	**(2)** Blockage, *m* = **0.091** Fr_h = 0.7 – 1.1	**(3)** Blockage, *m* = **0.110** Fr_h = 0.5 – 1.1
2.36 m	**(4)** Blockage, *m* = **0.062** Fr_h = 0.7 – 1.05	**(5)** Blockage, *m* = **0.077** Fr_h = 0.7 – 1.05	**(6)** Blockage, *m* = **0.093** Fr_h = 0.7 – 1.05

The trends of soliton generation were investigated extensively with the largest blockage (Condition 3) to provide the most prominent representations of solitons. Tests of this condition were carried out at Froude depth ranging from 0.5 to 1.1, with Fr_h increments varying from 0.1 at lower Froude depth to 0.025 surrounding the critical Froude depth region. The remaining conditions were carried out between Fr_h = 0.7 and 1.05 or 1.1 with increments of 0.05 between Fr_h = 0.9 and 1.05 or 1.1, resulting in a higher concentration of data near the critical region.

2.2 Advanced Model Techniques

When recording a phenomenon that is directly involved with the free surface, glare is increased and contrast is reduced by bright lighting and reflective water surfaces, causing footage to be ambiguous and hard to interpret. To reduce glare and increase contrast, only the light that is necessary must be used. An innovative method of ensuring only what is required to be illuminated is the use of fluorescence and ultraviolet (UV-A) lighting, otherwise referred

to as 'black lighting'. Most objects absorb ultraviolet light radiation, causing them to remain dark when exposed to UV-A lighting. However, if a 'phosphor', such as fluorescent paint or rhodamine dye is illuminated by UV-A lighting, the light will be reflected, causing the phosphor to glow brightly (Physics.org, 2016).

Fluorescent paint was applied to the external surface of the ship model to ensure the model was clearly visible and model responses could be observed. Positively buoyant, fluorescent wax particles were applied to the water, creating a fluorescing layer on the free-surface. Rhodamine dye is a phosphor and mixes when placed in water, therefore a large amount will cause an entire fluid domain to illuminate under UV-A lighting. A static array of seven UV-A flood lamps were positioned to illuminate the free-surface and model in critical regions where footage was recorded. A single UV-A flood lamp was fixed to the moving carriage powered by a 12V battery causing the area ahead of the carriage to remain under constant illumination.

Multiple high-definition GoPro 'Hero 4' recording devices were fixed to the carriage in various locations providing optimal angles to capture solitons and the dynamic vessel response. All recording devices were remotely operated and synchronised to allow for multiple perspectives in the video.

2.3 Error Analysis

To ensure consistent and valid results, and to quantify the sensitivity and repeatability of soliton generation repeat runs were conducted at $m = 0.073$ for $Fr_h = 1.0$. The standard deviations for each parameter each was computed using the mean value from time series data at steady speed. The water surface elevation values are taken from the maximum soliton amplitude recorded at WP3, anecdotal evidence suggests that the typical standard deviation for the particular wave probes is approximately 2-4% (Macfarlane, 2016). The standard deviation was calculated using Equation (2), where X takes on each value in the set, $\bar{X}$ is the average of the entire set and n is equal to the number of values.

$$Std.Dev. = \sqrt{\sum \frac{(X - \bar{X})^2}{(n-1)}} \tag{2}$$

Table 2: Calculated standard deviation of measured parameters

Recorded Parameter	Model Speed	WSE	Mean Drag	Fwd. Sinkage	Aft Sinkage
Standard Deviation	**± 0.13 %**	**± 0.14 %**	**± 0.83 %**	**± 0.66 %**	**± 5.1 %**

Due to the standard deviation of aft sinkage, error bars have been applied to trim data, a product of forward and aft sinkage, with a cumulative standard deviation of 5.8%.

3 Results and Discussion

The results of physical scale model testing may be separated into two distinct sections; the water surface elevation, defining the solitons, and the vessel response due to soliton generation. The solitons were analysed using data acquired from the static wave probes, and the vessel responses were analysed using data acquired from the carriage mounted instrumentation; the forward and aft LVDT's and the load cell.

3.1 The Effect of Blockage on Soliton Generation

Solitons were visually observed from a Froude depth of 0.7, and as Froude depth increased the solitons became visibly larger as the speed and energy being forced into the water increased. Figure 4 illustrates the water surface elevation for an equivalent blockage coefficient and increasing speed recorded by the three static wave probes placed 3.5m lengthwise along the channel. The leftmost plots are the water surface elevation recorded by Wave Probe 1 (WP1), located approximately 13m from the carriage start, the middle plots by WP2, a further 3.5m downstream and the rightmost by WP3, approximately 5m from the carriage end. For reference, the aft of the ship model would be positioned approximately at the zero-down-crossing point immediately following the body of water containing the solitons that preceded the model, hereafter termed the 'surge wave'. For example, at $Fr_h = 0.7$ (Figure 4a) this occurs at approximately 20.3 seconds for WP1; 24.3s for WP2 and 28.4s for WP3.

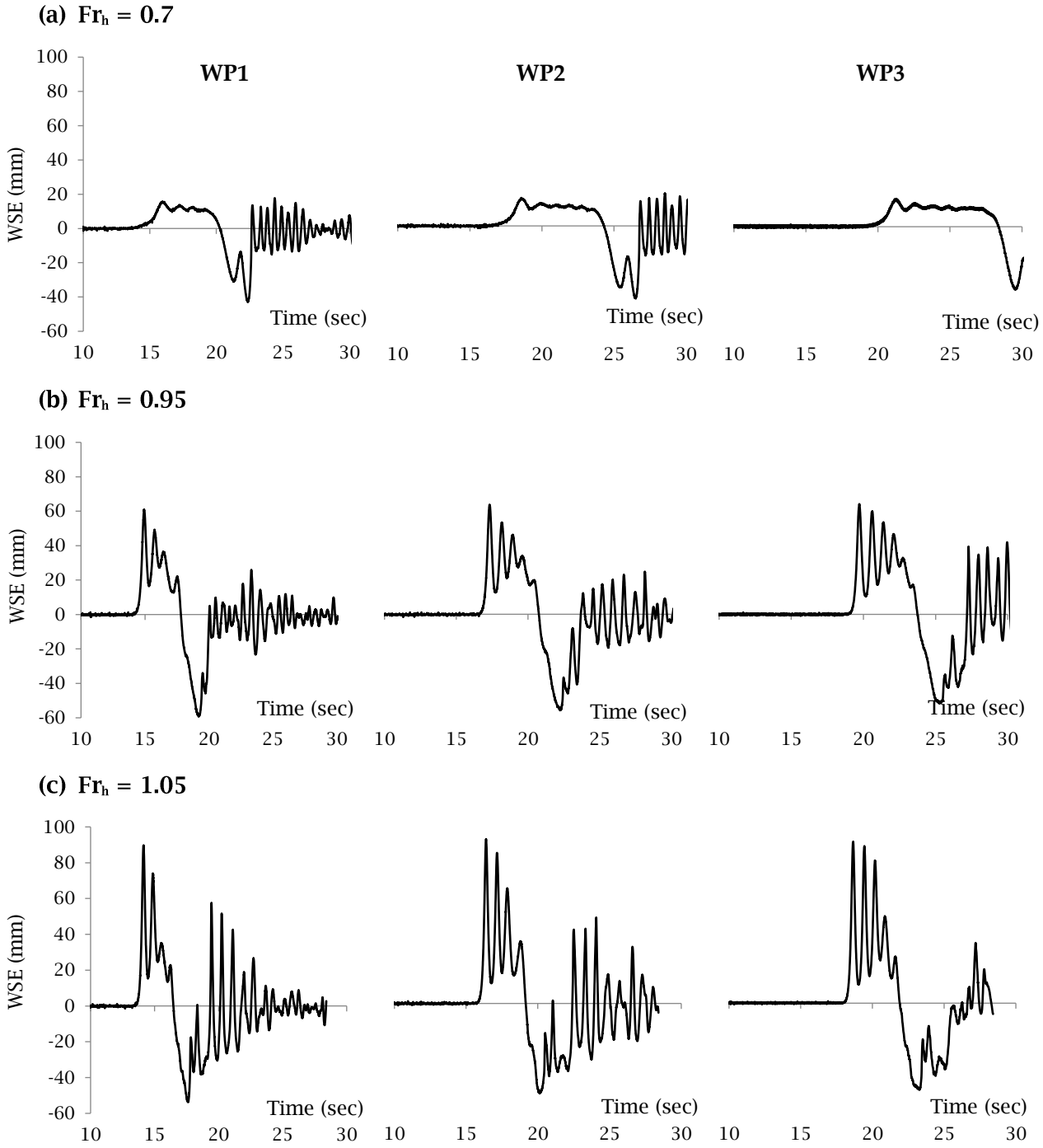

Figure 4: Water Surface Elevation (WSE) for blockage, *m* = 0.093. Left column = WP1, middle = WP2 and right = WP3 – (a) Fr_h = 0.7, (b) Fr_h = 0.95 and (c) Fr_h = 1.05

As Froude depth increases, corresponding to an increase in speed, the amplitude of the generated solitons increases. For example, the maximum wave height recorded at WP3 for a depth Froude number of 0.7 is approximately 14mm, at Fr_h = 0.95 this increases to 62mm and at Fr_h = 1.05 the maximum soliton amplitude exceeds 87mm, which is notably greater than half the water depth of 152mm. The continuous nature of soliton generation is represented by the growth of the surge wave, indicating solitons are an oscillation that will continue indefinitely if speed and channel conditions remain constant. At Fr_h = 0.7 the train of solitons begins to pass WP1 at approximately 15 seconds and a trough directly following the vessel passes shortly after 20 seconds. Upon reaching WP3, the first soliton begins to pass at ~20 seconds and the trough passes at ~28 seconds.

The solitons contained within the surge wave preceding the vessel have peaks and troughs with a local mean water line for the solitons which are further developed. Figure 5 illustrates the section of the water surface elevation as solitons pass WP3 for $Fr_h = 0.95$ and $Fr_h = 1.05$ in Figure 4b and Figure 4c respectively, sharing a common, arbitrary t = 0 point for comparison. The average values between the peak and following trough demonstrate the local soliton mean water line, levelling towards horizontal as more solitons are developed in a soliton train.

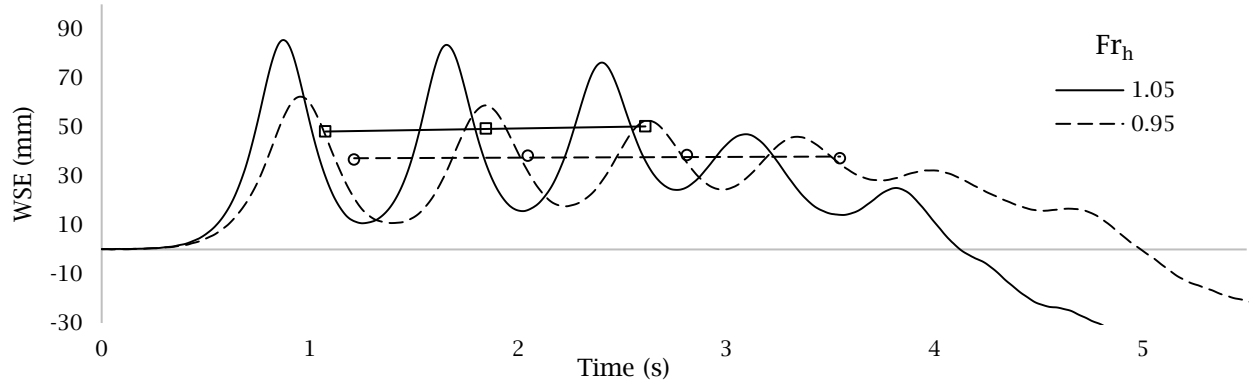

Figure 5: Water Surface Elevation (WSE) for blockage, $m = 0.093$ at $Fr_h = 0.95$ and $Fr_h = 1.05$ illustrating local mean water line of solitons

It is evident that the faster model speed of $Fr_h = 1.05$ generated solitons that are larger in peak amplitude, although the troughs are at a similar height above the still water line. This results in a larger local mean water line amplitude of the surge wave. It is also clear the solitons generated by the model travelling at $Fr_h = 1.05$ are travelled faster, giving a steeper appearance, and had a lower period of incidence past the wave probe.

To explore the influence of blockage on soliton generation further tests of a similar nature were performed with systematic variation of model draft and channel width and the raw time-series data was analysed to extract the peaks of soliton amplitude. Increasing the Froude depth number was achieved by increasing the vessel speed as depth was fixed at 152mm. Figure 6 is a representation of the maximum soliton peak amplitude recorded at WP3, which was typically the first soliton to pass the wave probe. The soliton amplitude was made dimensionless by dividing by the water depth, and is plotted for increasing Froude depth number for each of the six blockage conditions outlined in Table 1.

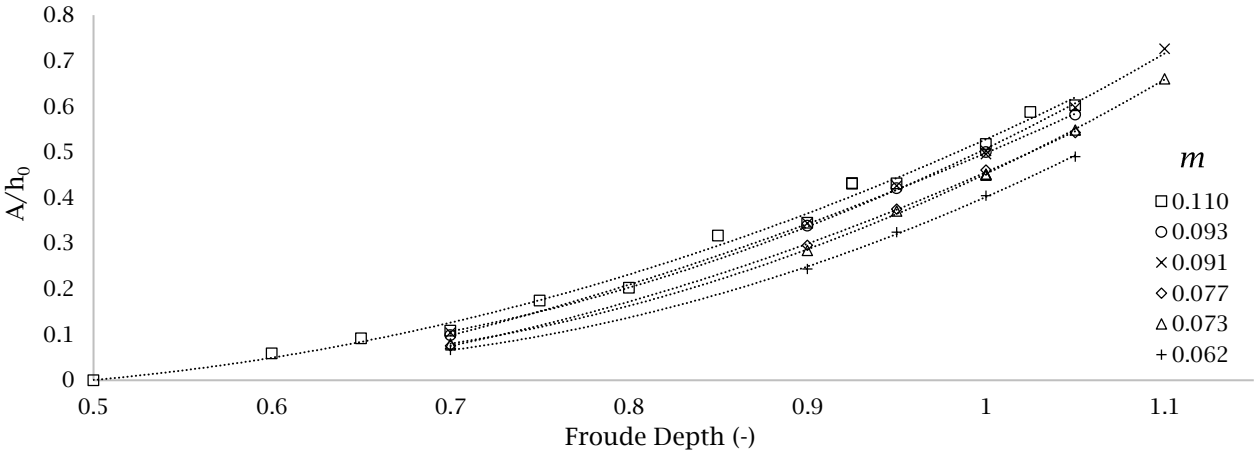

Figure 6: Soliton amplitude as a function of Froude depth for varying blockage

The first instance of a soliton, although quite insignificant with an amplitude of ~9mm, was generated at $Fr_h = 0.6$ for $m = 0.1096$. For all conditions tested, as the Froude depth increased beyond 0.7 soliton amplitude increased at a cumulative rate. Soliton amplitude is dependent also on blockage as deeper vessel draft results in more energy being transferred into the water and decreased channel width contains the energy in a smaller cross-section. Figure 7 illustrates the maximum soliton amplitude recorded at WP3 for increasing blockage at various Froude depths.

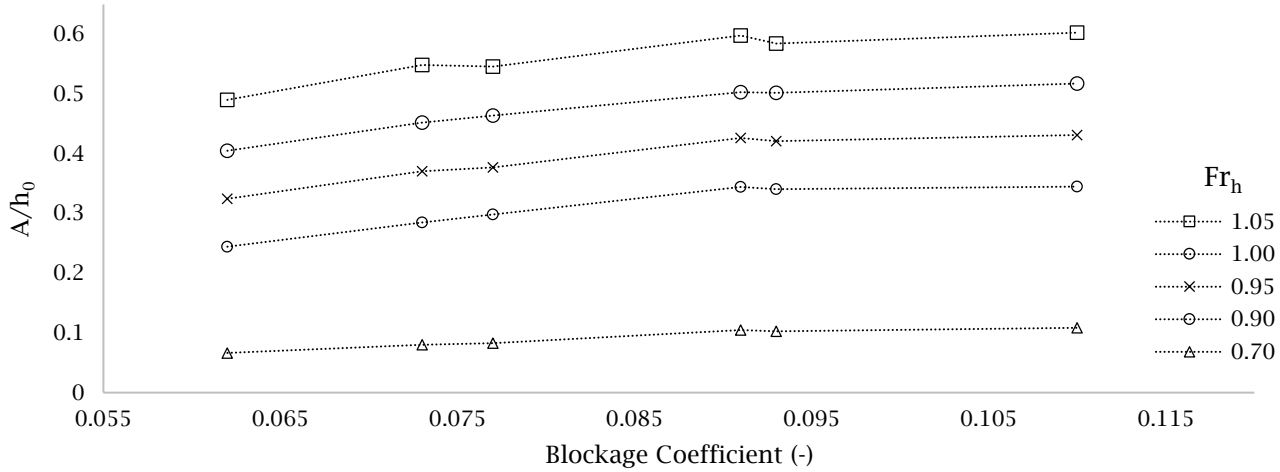

Figure 7: Soliton amplitude as a function of blockage for varying Froude depth

Generally, increasing blockage coefficient for equivalent Froude depth produces an increase in soliton amplitude, however for Froude depths approaching critical, the slightly larger blockage does not respond with slightly larger soliton amplitude. To investigate further, the nominally equivalent blockage pairs at m = 0.073 and 0.077, and m = 0.091 and 0.093 were compared at equivalent Froude depths.

Figure 8 provides a visual representation of the cross-section of blockages varied by model draft and channel width, the diagrams have been drawn to scale for accurate visual representation.

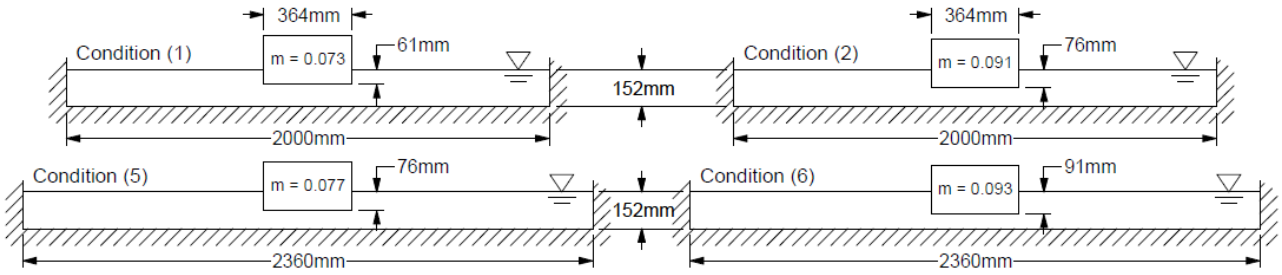

Figure 8: Scale cross-sections of varying blockage coefficients

The dimensionless soliton amplitude for the nominally equivalent blockages is represented in Figure 9 for increasing Froude depth.

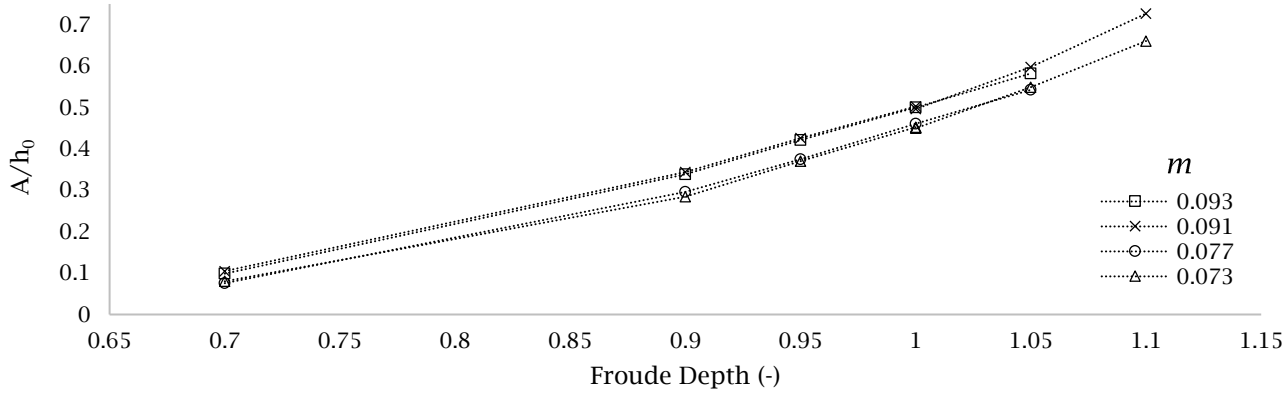

Figure 9: Soliton amplitude for nominally equivalent blockages at varying Froude depth

Similar to witnessing the soliton event for comparable blockages, the soliton response is indistinguishable. There is little difference between the pairs of nominally equivalent blockages, and only upon inspection of the measured data

do trends become clear. Table 3 is a quantitative comparison between the difference in vessel draft, channel width and blockage, and the average difference between the soliton amplitude measured for each Froude depth number.

Table 3: Soliton amplitude comparison of nominally equivalent blockages

#	*T* (mm)	*b* (m)	*m*	#	*T* (mm)	*b* (m)	*m*
(1)	61	2.00	**0.073**	(2)	76	2.0	**0.091**
(5)	76	2.36	**0.077**	(6)	91.5	2.36	**0.093**
%	**21.90**	**16.51**	**5.46**	***%***	**18.51**	**16.51**	**1.96**
Average Amplitude % Difference			**2.3**	**Average Amplitude % Difference**			**-1.3**

It is evident increasing blockage does not correspond with an equivalent increase in soliton amplitude. For nominally equivalent blockage of ~0.092 the larger blockage averages a smaller soliton amplitude. The discrepancy between the difference in blockage and the difference in soliton amplitude is ~3% in favour of the smaller blockage for both pairs of conditions. If the difference was equal to zero, blockage could be suggested to define soliton amplitude regardless of model draft or channel width. However, this is not the case, suggesting the narrower channel width at m = 0.073 and 0.091 has a greater influence than the deeper draft at m = 0.077 and 0.093. Figure 10 presents soliton amplitude for increasing model draft at the two channel widths width a Fr_h = 1.

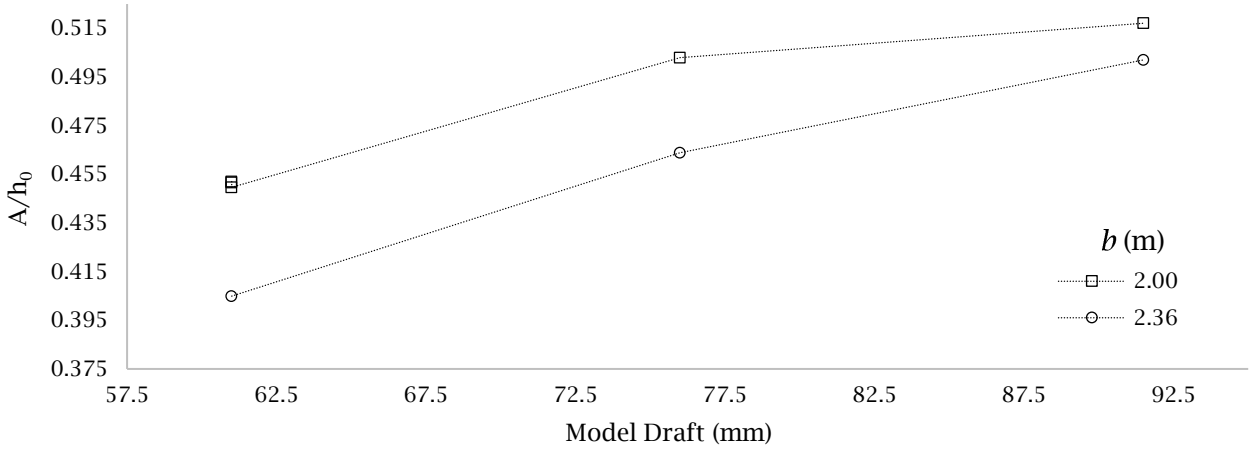

Figure 10: Soliton amplitude for increasing model draft at varying channel widths for Fr_h = 1.0

The difference in influence between vessel draft and channel width is difficult to interpret, however for both model draft and channel width the values of soliton amplitude appear to converge towards an approximately similar value This is likely due to restrictions of the water depth; as blockage increases, soliton amplitude for a given water depth will approach a maximum, and increasing the vessel draft and reducing the channel width will not result in an increase in soliton amplitude, suggesting a maximum soliton amplitude to water depth ratio.

An important function of solitons is that their amplitude governs their speed. As soliton amplitude increases, the speed of the wave, *v*, also increases for constant water depth, *h*, (3), (Remoissenet, 2013).

$$v = \sqrt{g(h+A)} \tag{3}$$

As increasing amounts of energy are transferred into the channel as blockage increases, the soliton amplitude and speed increase, and the time taken for each soliton to pass the wave probe, hereafter termed the period of incidence, T_f will decrease. The time difference between soliton peaks was obtained from wave probe data to determine T_f for each run. T_f was converted to a moving-reference period of generation, $T_{m;}$ for the model travelling at speed, *U;* producing solitons with wave celerity, *c;* Equation (4) (Ertekin et al., 1984).

$$T_m = \left[c/(c-U)\right]T_f \tag{4}$$

Figure 11 illustrates the period of soliton generation for increasing blockage coefficient. The two channel widths for two Froude depth numbers are presented as separate trends to demonstrate the effect channel width and model draft have on the period of soliton generation.

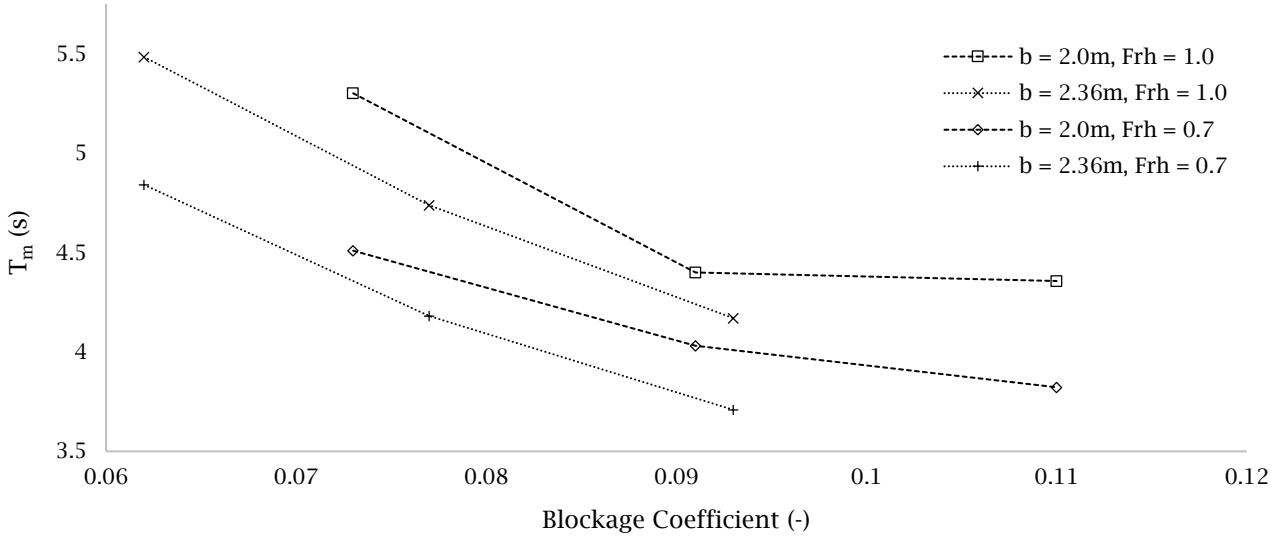

Figure 11: Soliton period of generation as a function of Froude depth for varying channel widths as blockage increases

As blockage increased, the period of soliton generation decreased, however as Froude depth increased, the frequency of soliton generation increased. It is also evident that the period of soliton generation was not defined by blockage to the same degree as soliton amplitude. For nominally equivalent blockages at equivalent Fr_h the period of generation was lower for blockage with wider channel width and deeper model draft. It is therefore suggested that model draft has a more significant effect than channel width when considering the frequency solitons are generated, and period is not considered an explicit function of blockage.

As soliton amplitude and period of generation vary depending on the operating conditions of the model and the surroundings, the model itself responded to generating solitons, typically with a period equal to that of soliton generation.

3.2 Vessel Response during Soliton Generation

Similar to a vessel travelling at Froude depth critical speed in open water encountering a peak in trim and resistance, the model underwent substantial increases in trim and resistance, however the peaks were oscillatory with a period equal to that of soliton generation. The beginning of the vessel response at critical Froude depth is comparable between open water and a confined waterway; a vessel travelling in open water at critical Froude depth will 'climb its own bow wave', experiencing an increase in trim. The model travelling in a confined water also underwent an increase in trim as the bow wave increased, however as a soliton propagated forward away from the vessel, the trim reduced. In ideal circumstances this cycle would continue indefinitely with the generation of each soliton. Model resistance also fluctuated cyclically corresponding to soliton generation; as energy was forced into a developing soliton the resistance peaked, and subsequently subsided as a soliton left the bow. A time-series of a single test run is given in Figure 12, illustrating a representation of dynamic trim.

Dynamic trim was calculated from the difference between forward and aft sinkage recorded with the LVDT's as the model travelled the length of the channel. Dynamic trim and model speed are plotted against the model's longitudinal position relative to the carriage start for a blockage coefficient of m = 0.093 and a Froude depth of 1.05. The model accelerates between 0m and 2m and begins decelerating at 20m. The recorded period of generation calculated from wave probe data for the condition presented in Figure 12 was 4.7 seconds, at $1.27ms^{-1}$ (Fr_h = 1.05) a soliton was produced every 5.9m, correlating with a single oscillation in the following figures.

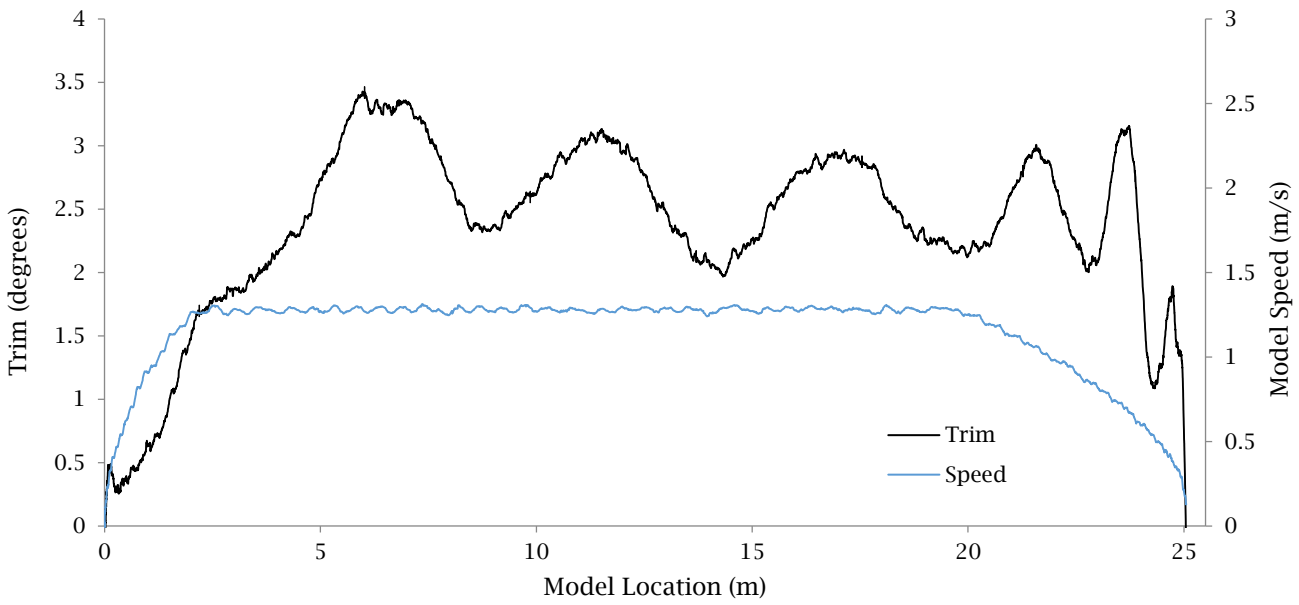

Figure 12: Dynamic trim and model speed plotted against model longitudinal location for m = 0.093 at Fr_h = 1.05

The fluctuations of trim are immediately obvious, upon reaching steady speed the model began producing solitons as reflected by the cyclic changes in trim response, which continued to be generated until the model began decelerating. The first soliton to be generated has unsteady effects due to the acceleration of the model, and as the model progressed the trim oscillations appear to approach a consistent trend which could be explained as a 'steady-state' oscillation, meaning that each cycle is indistinguishable from the one that precedes it. If the model was to continue to travel at constant speed in a longer testing facility this would likely be confirmed.

A quantitative measure of the amplitude of dynamic trim is to measure the difference between a trim peak and the following trough. Due to the acceleration-induced unsteadiness of the first trim cycle, the value of the dynamic trim peak and following trough of the second soliton-induced fluctuation was acquired from time-series trim data. The oscillatory dynamic trim difference is presented in Figure 13 for increasing Froude depth for each condition.

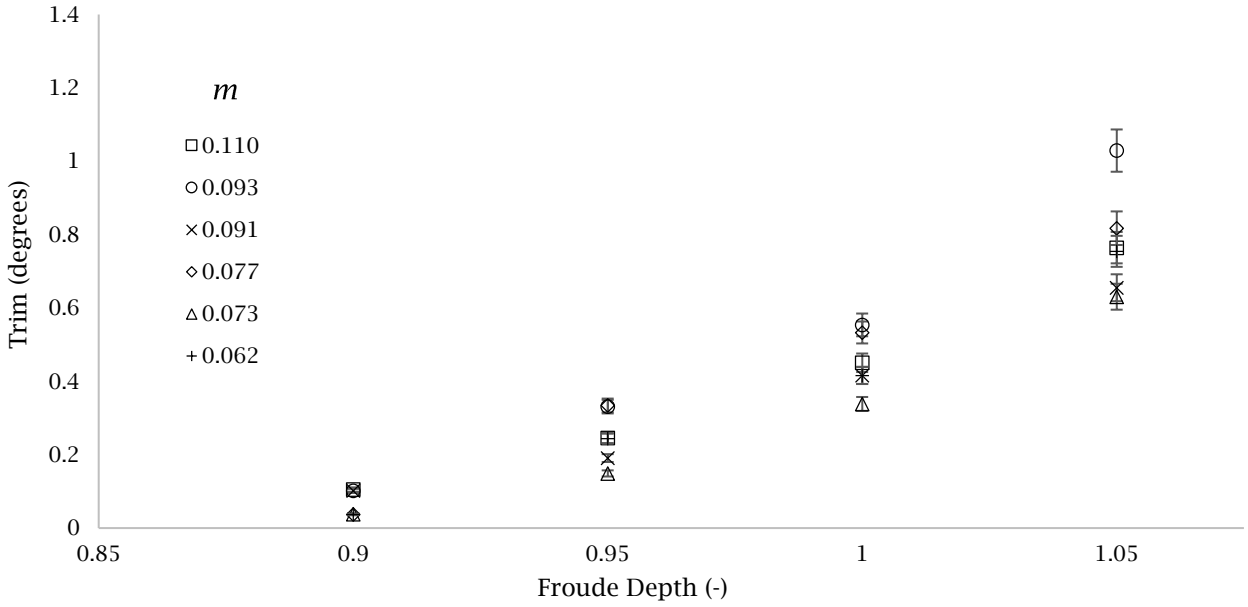

Figure 13: Trim difference during cyclic soliton generation for varying blockage

As Froude depth increased, dynamic trim oscillations increased with a similar trend to soliton amplitude illustrated in Figure 6, suggesting a correlation. It is not only the trim that oscillated with a period equal to that of soliton

generation, resistance also fluctuated as each soliton generated and subsequently dispersed from the bow of the model. An extract of the data provided in Figure 12 is presented in Figure 14, encompassing the consistent peaks of dynamic trim including resistance recorded from the load cell between 9m and 19.5m, a region of steady speed. The resistance values were made dimensionless by dividing the resistance force, F, in kilograms by model displacement, Δ in kilograms.

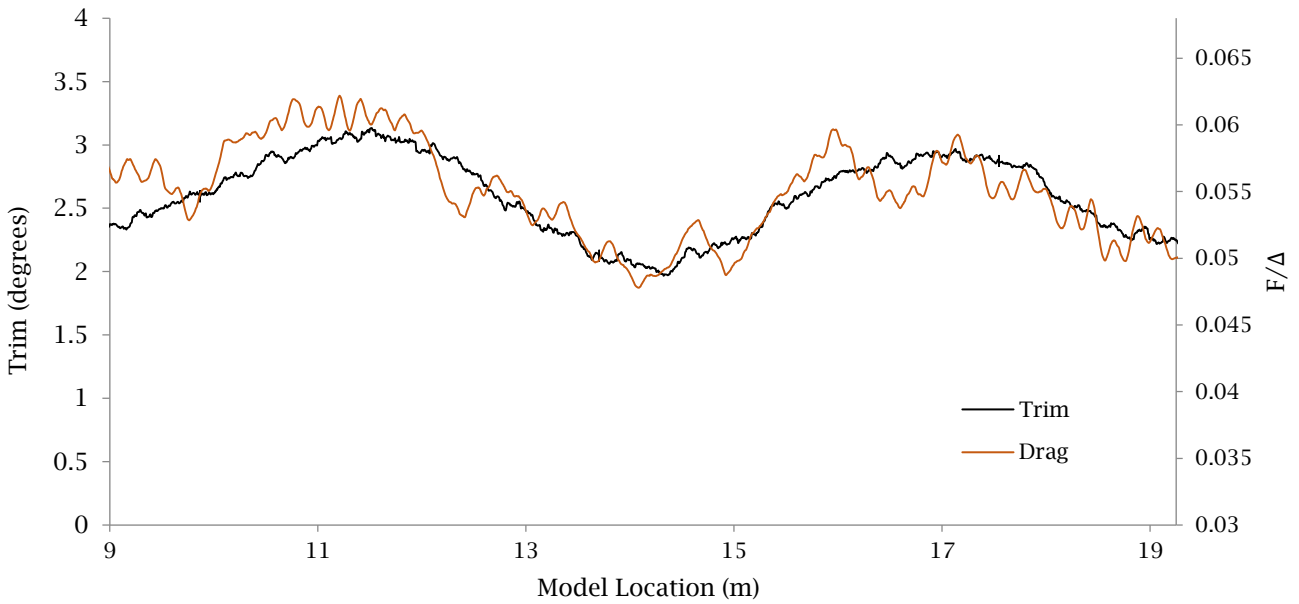

Figure 14: Dynamic vessel trim and resistance during soliton generation: blockage, *m* = 0.093 at Fr_h = 1.05

The similarity in response for trim and resistance is coincident indicating that the dynamic trim and resistance both fluctuated with a period equal to that of soliton generation.

Increasing model draft increases the viscous or 'frictional' drag due to increased wetted surface area and also increases the pressure or 'wave-making' resistance. Therefore, resistance would be expected to increase as vessel draft increased. Considering the resistance fluctuates about a mean, the average resistance whilst at steady-state speed offered comparable values of resistance for each condition. Figure 15 is the average dimensionless resistance force measured between longitudinal vessel locations of 5m and 15m for increasing Froude depth for each of the conditions tested.

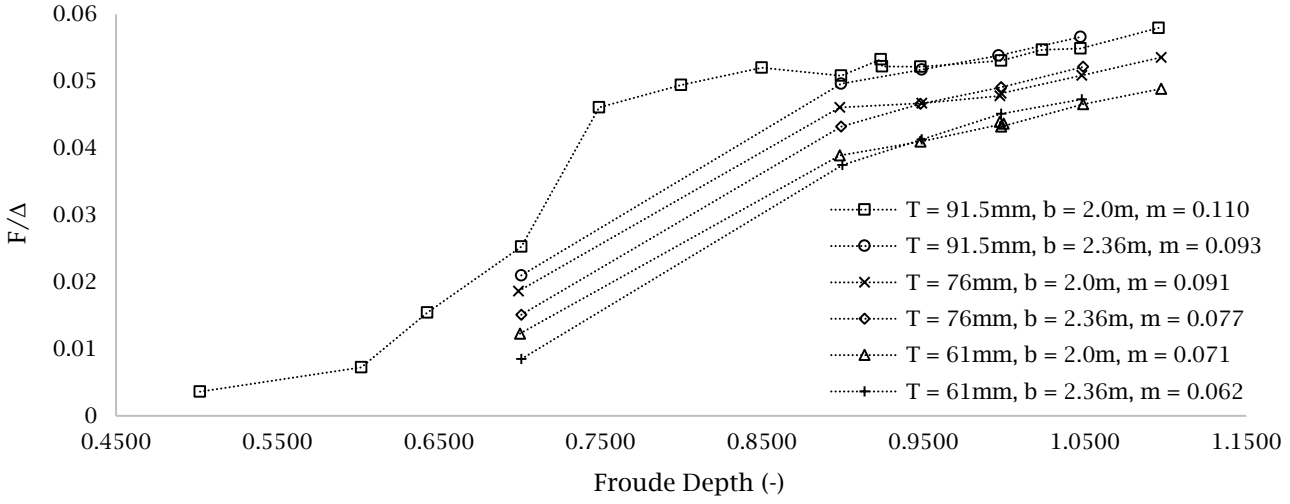

Figure 15: Measured resistance force for increasing Froude depth at varying blockage

A correlation exists between model resistance and the findings of wave cusp angle by Havelock (1908). The rate of resistance increase began to accelerate beyond approximately Fr_h = 0.6, when wave angle is known to begin

diverging, and dramatically increased beyond Fr_h = 0.7. However, resistance only dramatically increased until Fr_h = 0.75, upon returning to a gradual and steady increase due to increasing speed. Comparably between blockages, at Fr_h = 0.7, the resistance increased for increasing draft and decreasing channel width, this is also evident at Fr_h = 0.9, however values for equivalent drafts approached a common value. At Fr_h = 0.95 the resistance converged to a nominally equivalent value for each vessel draft, although soliton amplitude was greater for the condition with a narrower channel width and increased blockage, suggesting an independence of channel width at Fr_h = 0.95. Interestingly, beyond Fr_h = 0.95 resistance was slightly lower for each model draft with narrower channel width, even though blockage and soliton amplitude were larger. Although slightly less energy was being transferred into the water due to the recorded wave-making resistance, the results suggest that the containment of energy due to channel width is what attributed to the soliton amplitude increase. As expected the resistance increased as model draft increased, indicating an increase in frictional and wave-making resistance.

3.3 Advanced Model Techniques

A subsequent aim of this study is the creation of a web-based educational multimedia tool drawing on both the physical measurements presented in the previous section and video footage acquired using advanced and novel techniques.

To capture footage suitable for web-based media presentation, the footage must be easy to interpret and any ambiguities due to glare and reflections must be removed, especially for a complex phenomenon such as solitons. A simple method of minimising glare and increasing contrast is to reduce the number of light sources, especially overhead light as shadows necessary for defining the wave free surface are eliminated by overhead light. Adding fluorescing media to the model and water illuminated with UV-A lighting resulted in only the model and free-surface reflecting light. The progression of lighting techniques can be seen in Figure 16, where three different methods are shown for the same experimental condition. The leftmost plot is the typical lighting arrangement for the Model Test Basin, the middle plot is a result of using only the perimeter lighting, and the rightmost plot is fluorescing media illuminated by UV-A lighting.

Figure 16: Representation of equivalent soliton condition captured using various lighting effects

The results are obvious; a typical lighting arrangement allows the surface to be defined by the distortion of the bright reflections of the overhead lights, however it is difficult to define solitons. The amplitude and form of the solitons can be roughly estimated from the left channel wall. Reduced direct lighting offers a much clearer representation, it is clear there are two solitons which are perpendicular to the sailing line, and the wave elevation can be estimated by looking to the channel wall. When fluorescing, the two solitons are clearly defined, the slope of the waves can be estimated by the intensity of the light, and diverging waves are visible on the starboard side of the model. The speckled appearance is due to the layering of the fluorescent wax particles.

Using multiple GoPro Hero 4 high-definition recording devices mounted to the vessel in various locations, footage was captured to synthesise into a web-based educational tool. Computer-generated imagery and footage demonstrates the implications of vessels operating at speeds approaching critical Froude depth, expressing the need to avoid the condition or to pass through as fast as practicable.

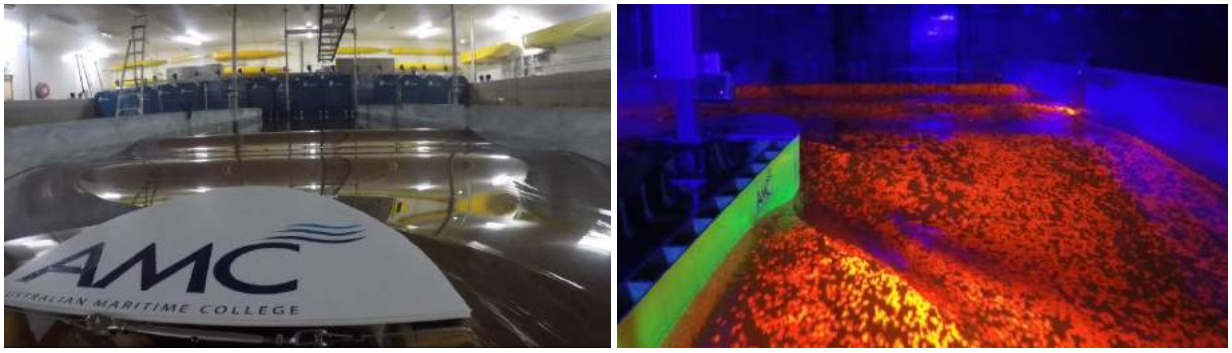

Figure 17: Vessel mounted perspective of soliton generation

4 Concluding Remarks

Physical scale model tests were conducted to explore the governing influence of blockage coefficient and the components that comprise it upon the generation of solitons and the model response. It was determined that a nominally equivalent blockage coefficient for an equivalent Froude depth resulted in an observably indistinguishable soliton amplitude, however, upon closer inspection the solitons were not identical. Regardless of how blockage was comprised, soliton amplitude converged towards a maximum amplitude defined by the water depth as Froude depth and blockage increased. The period of soliton generation was not explicitly defined by blockage, and the draft of the model had a more significant influence than channel width. The continuous train of solitons generated by the model was contained in a body of water or 'surge wave' that preceded the model with a local mean water line that was greater than the still-water line. This wave grew in length and number of solitons as the model continued to operate at a soliton-generating Froude depth.

The dynamic trim and resistance of the vessel oscillated with a period equal to that of soliton generation and the difference between local peaks and troughs of dynamic trim oscillations increased with blockage comparably to soliton amplitude. Also the trends of average model resistance exhibited correlation with the divergence of wave cusp angle. A longer test facility would have allowed oscillations in trim and resistance to reach a continuous state of generation and each fluctuation would be indistinguishable from the last. As vessel draft increased, model wave-making resistance and consequently soliton amplitude increased. However, near critical Froude for equivalent model draft, when channel width was reduced the resistance remained largely unchanged, however soliton amplitude continued to increase, suggesting the channels containing the wave energy caused soliton amplitude to increase.

In the absence of readily available soliton demonstration, footage of physical scale model testing recorded with multiple vessel mounted recording devices was synthesised into a multimedia presentation with the intention of accessible education. Advanced qualitative techniques in the form of fluorescent paint, positively buoyant wax particles and rhodamine dye illuminated by ultraviolet (UV-A) lighting provided a visually enhanced demonstration of the soliton event. These techniques are applicable to any investigations conducted with a direct interest in the free surface, especially to capture an unambiguous representation of wave patterns.

5 Future Works

Blockage can be varied by more factors than those that could be investigated in this study; hull cross sectional geometry, water depth and geometry of the channel such as sloping banks contribute to blockage and therefore will affect the generation and form of solitons. The effect sloping banks has on soliton generation is worthy of investigation as this would be typical of the majority of restricted waterways.

It was shown that the surge wave preceding the vessel contained a train of solitons with a raised local mean water line and this is likely to correspond to the increase in energy required to maintain critical speed and may be worthy of further investigation. Resistance increased whilst generating solitons, and the body of water preceding the vessel increases in length and number of solitons as the vessel continues at soliton-generating speed. A correlation would likely be found between the increased wave-making energy transferred into the water and the energy of the surge wave.

Acknowledgements

The author would like to thank the guidance and expertise of supervisor Gregor Macfarlane, inspiration of Adjunct Associate Professor Alex Robbins (*FIGJAM)*, the invaluable assistance and cooperation of AMC staff, particularly Adam Rolls, Kirk Meyer, Liam Honeychurch and Tim Lilienthal. As well as the irreplaceable support of family, valuable discussions with fellow peers and funding from the Australian Research Council through their Linkage program (LP150100502).

References

Dand, I., Dinham-Peren, T., & King, L. (1999). Hydrodynamic aspects of a fast catamaran operating in shallow water. *Hydrodynamics of High Speed Craft. The Royal Institution of Naval Architects, London, 117*.

Ertekin, R., Webster, W., & Wehausen, J. (1984). *Ship-generated solitons*: Office of Naval Research, Fluid Dynamics Branch.

Ertekin, R., Webster, W., & Wehausen, J. (1985). Waves caused by a moving disturbance in a shallow channel of finite width. *Journal of Fluid Mechanics, 169*, 275-292.

Geerts, S., Van Kerkove, G., Vantorre, M., & Delefortrie, G. (2011). Waterline registration using fluorescent lighting. *Advanced Model Measurement Technology for EU Maritime Industry*, 61-69.

Gourlay, T. (2010). Hydrodynamic effects on fast monohulls or catamarans travelling through the critical speed in shallow water. *2010, 51*, 18. doi:10.0000/anziamj.v51i0.2635

Havelock, T. H. (1908). The propagation of groups of waves in dispersive media, with application to waves on water produced by a travelling disturbance. *Proceedings of the Royal Society of London. Series A, Containing Papers of a Mathematical and Physical Character, 81*(549), 398-430.

Macfarlane, G. (2012). *Marine Vessel Wave Wake: Focus on Vessel Operations with Sheltered Waterways.* (Doctor of Philosphy), University of Tasmania, Australian Maritime College.

Macfarlane, G. J., Bose, N., & Duffy, J. T. (2014). Wave wake: focus on vessel operations within sheltered waterways. *Journal of Ship Production and Design, 30*(3), 109-125.

Macfarlane, G.J. Personal communication, 24th February, 2016, Discussion of the current knowledge of solitons in the wider community. Australian Maritime College.

Macfarlane, G.J. Personal communication, 29th September, 2016, Discussion of typical expected errors of Model Test Basin Equipment. Australian Maritime College.

MAIB. (2000). *Report on the investigation of the man overboard fatality from the angling boat Purdy at Shipwash Back, off Harwich on 17 July 1999*. Retrieved from Southampton:

Physics.org. (2016). How do black (UV) lights work? *Physics.org*.

Remoissenet, M. (2013). *Waves called solitons: concepts and experiments*: Springer Science & Business Media.

Robbins, A., Thomas, G., Renilson, M., MacFarlane, G., & Dand, I. (2009). Vessel trans-critical wave wake, divergent wave angle and decay. *Royal Institution of Naval Architects. Transactions. Part A. International Journal of Maritime Engineering, 151*(2), 25-38.

Robbins, A., Thomas, G., Renilson, M., Macfarlane, G., & Dand, I. (2011). Subcritical Wave Wake Unsteadiness. *International Journal of Maritime Engineering, 153*(A3), A153-A171. doi:10.3940/rina.ijme.2011.a3.201

Roseman, D. P. (1987). The MARAD systematic series of full-form ship models.